Efficient Blue Light-Emitting Diodes Based on Triarylamine-Substituted Dipyrazolopyridine Derivatives

Y. T. Tao,*[,†,‡] C. H. Chuen,[†] C. W. Ko,[†] and J. W. Peng[‡]

Institute of Chemistry, Academia Sinica, Taipei, Taiwan, Republic of China, and Department of Chemistry, National Tsing-Hua University, Hsin-chu, Taiwan, Republic of China

Received March 22, 2002. Revised Manuscript Received August 13, 2002

A new series of highly luminescent dipyrazolopyridine dyes carrying a triarylamine substituent were synthesized and evaluated as light-emitting materials in electroluminescent devices. Double-heterojunction devices with 4,4′-bis[*N*-(1-naphthyl)-*N*-phenylamino]biphenyl as the hole-transporting layer, these dipyrazolopyridine dyes as the emitting layer, and tris-(8-hydroxyquinoline) aluminum, or 1,3,5-tris(*N*-phenylbenzimidazol-2-yl)benzene, as the electron-transporting layer were fabricated. Highly bright blue or blue-green emission was obtained, depending on the emitting layer as well as the electron-transporting material used. A correlation between the electroluminescence behavior/device performance and the energy alignments of HOMO/LUMO energy levels of various layers is suggested.

Introduction

Light-emitting diodes (LEDs) using organic molecules (OLEDs) or organic polymers (PLEDs) are attracting a great deal of attention due to their application in flat panel displays. The progress has been fast and tremendous from the breakthrough in device fabrication[1] in 1987 and 1990, respectively, to the realization of commercial display applications[2] in recent years. The development in materials is pivotal in this technology. Depending on the role it plays in a device, the material has to function as an efficient charge transporter or an efficient light emitter or sometimes both. Morphology stability of various layers is another issue that needs to be addressed to have long enough operational lifetime for the devices.[3] Numerous fluorescent dyes and charge carriers have been developed in the past decade, yet the effort goes on in terms of color tuning, efficiency, and durability improvement. Besides the materials, a better understanding of the mechanism behind the light emission under various device configurations also greatly helps the construction of a more efficient device using the same materials. It usually takes the right combination of the electrodes, charge carriers, and emitters to achieve an optimized device.

For full color application, red, green, and blue (RGB) emission are required. An efficient blue emission is of particular interest because other colors can be down-converted from the blue emission. There are a number of efficient blue dyes developed in the past several years,[4−10] some of which possess reasonable or high glass transition temperature, T_g, a property suggested to be desirable for morphological stability reasons.[3] Recently, we reported a series of dipyrazolopyridine (PAP) derivatives to be very good blue-emitting materials in making electroluminescent (EL) devices.[11] However, many of the these PAP dyes do not exhibit a T_g so these dyes are only suitable for use as dopants in device fabrication. In this work, we are reporting a new series of dyes, 4-(4-diarylaminophenyl)-1,7-diphenyl-3,5-dimethyl-1,7-dihydrodipyrazolo[3,4-b;4′3′-e]pyridine (PAP-X), as the blue-emitting material in a multilayer EL device. Here, various diarylamino substituents were introduced in the para position of the 4-phenyl group (Figure 1) and were found to induce a T_g in these materials. The thermal, spectroscopic, and electrochemical properties were examined and the performances of double hetero-junction LED devices of the structures ITO/NPB/PAP-X/AlQ/Mg:Ag and ITO/NPB/PAP-X/TPBI/Mg:Ag, where NPB is 4,4′-bis[*N*-(1-naphthyl-1-)-*N*-phenylamino]biphenyl, AlQ is tris(8-hydroxyquinoline) aluminum, and TPBI is 1,3,5-tris(*N*-phenylbenzimidazol-2-yl)benzene, were measured. Highly bright blue or

* To whom correspondence should be addressed.
† Academia Sinica.
‡ National Tsing-Hua University.

(1) (a) Tang, C. W.; VanSlyke, S. A. *Appl. Phys. Lett.* **1987**, *51*, 913. (b) Burroughes, J. H.; Bradley, D. D. C.; Brown, A. R.; Marks, R. N.; Mackay, K.; Friend, R. H.; Burns, P. L.; Holmes, A. B. *Nature* **1990**, *347*, 539.

(2) See http://www.kodak.com/go/OLED and http://www.cdtltd.co.uk/.

(3) (a) Tokido, S.; Tanaka, H.; Noda, K.; Okada, A.; Taga, T. *Appl. Phys. Lett.* **1997**, *70*, 1929. (b) Han, E.; Do, L.; Niidome, Y.; Fujihira, M. *Chem. Lett.* **1994**, 969. (c) Fenter, P.; Schreiber, F.; Buloviæ, V.; Forrest, S. R. *Chem. Phys. Lett.* **1997**, *277*, 521.

(4) Hosokawa, C.; Higashi, H.; Nakamura, H.; Kusumoto, T. *Appl. Phys. Lett.* **1995**, *67*, 3853.

(5) Tao, X. T.; Suzuki, H.; Wada, T.; Sasabe, H.; Miyata, S. *Appl. Phys. Lett.* **1999**, *75*, 1655.

(6) Gao, Z.; Lee, C. S.; Bello, I.; Lee, S. T.; Chen, R.-M.; Luh, T.-Y.; Shi, J.; Tang, C. W. *Appl. Phys. Lett.* **1999**, *74*, 865.

(7) Tamoto, N.; Adachi, C.; Nagai, K. *Chem. Mater.* **1997**, *9*, 1077.

(8) Leung, L. M.; Lo, W. Y.; So, S. K.; Choi, W. K. *J. Am. Chem. Soc.* **2000**, *122*, 5640.

(9) Chan, L. H.; Yeh, H. C.; Chen, C. T. *Adv. Mater.* **2001**, *13*, 1637.

(10) Kim, Y. H.; Shin, D. C.; Kim, S. H.; Ko, C. H.; Yu, H. S.; Chae, Y. S.; Kwon, S. K. *Adv. Mater.* **2001**, *13*, 1690.

(11) (a) Balasubramanian, E.; Tao, Y. T.; Danel, A.; Tomasik, P. *Chem. Mater.* **2000**, *12*, 2788. (b) He, Z. Q.; Milburn, G. H. W.; Danel, A.; Puchala, A.; Tomasik, P.; Rasala, D. *J. Mater. Chem.* **1997**, *7*, 2323. (c) Danel, A.; He, Z.; Milburn, G. H. W.; Tomasik, P. *J. Mater. Chem.* **1999**, *9*, 339.

10.1021/cm020284h CCC: $22.00
Published on Web 09/13/2002

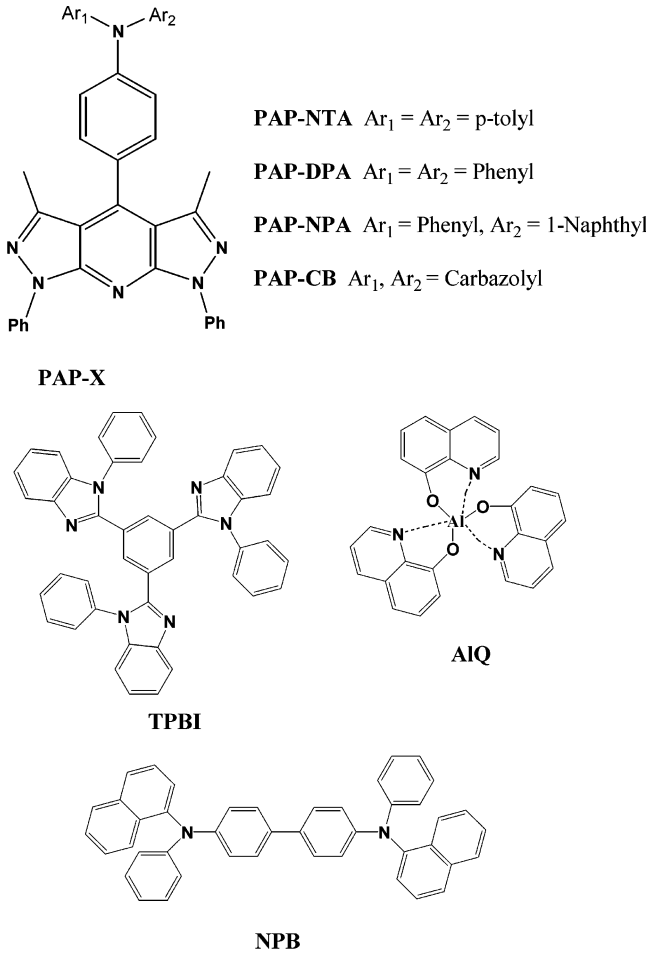

Figure 1. Structures of PAP-X derivatives and charge-transporting materials used in the study.

bluish-green emission was obtained. A substituent effect on the EL behavior and performance was observed. In particular, various amounts of emission from the electron-transporting layer (ETL) was found depending on the substituent. The effect on EL is understood in terms of the different charge mobility for different ETLs (AlQ or TPBI) and thus a subtle change in the charge recombination area. The substituent effect on the performance is explained by the energy level alignment of the highest occupied molecular orbital (HOMO) and lowest unoccupied molecular orbital (LUMO) of various layers and thus the barrier for charge crossing in the devices.

Experimental Section

General Information. NMR spectra were recorded on a Bruker AC 300 spectrometer. Absorption spectra were measured on a HP 8453 spectrometer. Emission spectra were obtained from a Hitachi F-4500 fluorimeter. DSC measurements were carried out on a Perkin-Elmer DSC7 calorimeter, with a heating rate of 20 °C/min under a nitrogen atmosphere. Cyclic voltammetric experiments were performed using a BAS 100B electrochemical analyzer. A three-electrode cell system with a glassy carbon, a platinum wire, and a silver wire as the working, counter, and reference electrode, respectively, was used. Freshly distilled, degassed dichloromethane was used as the solvent, with 0.1 M tetra-*n*-butylammonium hexafluorophosphate as the supporting electrolyte.

Materials. The various triaryl-substituted 1,7-diphenyl-3,5-dimethyl-1,7-dihydrodipyrazolo-[3,4-b;4′3′-e]-pyridines (PAP-X) were synthesized from 4-(4-bromophenyl)-1,7-diphenyl-3,5-dimethyl-1,7-dihydrodipyrazolo-[3,4-b;4′,3′-e]pyridine(PAP-Br) and the appropriate diarylamine by a palladium-catalyzed coupling reaction. Only the synthesis of PAP-NPA is described as a representative. The precursor PAP-Br was obtained from 5-amino-3-methyl-1-phenylpyrazole[12] and 4-bromobenzaldehyde according to the literature procedure.[13]

4-{4-[N-(1-naphthyl)-N-phenylaminophenyl]-1,7-diphenyl-3,5-dimethyl-1,7-dihydrodipyrazolo[3,4-b;4′3′-e]pyridine (PAP-NPA). A mixture of 4-(4-bromophenyl)-1,7-diphenyl-3,5-dimethyl-1,7-dihydrodipyrazolo[3,4-b;4′,3′-e] pyridine (1 g, 2 mmol), 1-naphthylphenylamine (444 mg, 2 mmol), sodium *tert*-butoxide (292 mg, 3 mmol), and palladium(II) acetate (5.4 mg, 0.024 mmol) was placed in a round-bottom flask and purged with nitrogen. Forty milliliters of dry toluene was added. To the solution was added tri-*tert*-butylphosphine (0.015 mL, 0.06 mmol) and the solution was brought to reflux. The reaction was followed by TLC until the starting material was all consumed. Upon cooling to room temperature, solid precipitates appeared. A small amount of water was added and the mixture was stirred for another 30 min. The precipitates were collected and washed with water and ethyl acetate to yield the crude product (1.02 g, ∼80%). Further purification by gradient sublimation afforded the material used for OLED fabrication. mp 279−280 °C. ^{1}H NMR (δ, $CDCl_3$): 2.23 (s, 6H), 7.03−7.08 (t, 1H), 7.11−7.15 (d, 2H), 7.20−7.33 (m, 8H), 7.36−7.44 (m, 2H), 7.48−7.56 (t, 6H), 7.81−7.84 (d, 1H), 7.92−7.98 (t, 2H), 8.39−8.42 (d, 4H). FAB mass (*m*/*z*): 632 (M^+). Anal. Calcd for $C_{43}H_{32}N_6$: C, 81.62; H, 5.10; N, 13.28. Found: C, 81.37; H, 4.96; N, 13.30%.

4-[4-(di-p-tolylaminophenyl)]-1,7-diphenyl-3,5-dimethyl-1,7-dihydrodipyrazolo[3,4-b;4′3′-e]pyridine (PAP-DTA). Yield 72.8%. mp 246−248 °C. ^{1}H NMR (δ, $CDCl_3$): 2.26 (s, 6H), 2.35 (s, 6H), 7.08−7.18 (m, 10H), 7.25−7.30 (t, 4H), 7.51−7.56 (t, 4H), 8.40−8.43 (d, 4H). FAB mass (*m*/*z*): 610 (M^+). Anal. Calcd for $C_{41}H_{34}N_6$: C, 80.63; H, 5.61; N, 13.76. Found; C, 80.73; H, 5.55; N, 13.80%.

4-[4-(N,N-diphenylaminophenyl)]-1,7-diphenyl-3,5-dimethyl-1,7-dihydrodipyrazolo[3,4-b;4′3′-e]pyridine (PAP-DPA). Yield: 73.4%. mp 247−248 °C. ^{1}H NMR (δ, $CDCl_3$): 2.26 (s, 6H), 7.11−7.14 (t, 2H), 7.18−7.37 (m, 14H), 7.50−7.56 (t, 4H), 8.39−8.43 (d, 4H). FAB mass (*m*/*z*): 582 (M^+). Anal. Calcd for $C_{39}H_{30}N_6$: C, 80.39; H, 5.19; N, 14.42. Found: C, 80.43; H, 5.18; N, 14.73%.

4-[4-(N-carbazolylphenyl)]-1,7-diphenyl-3,5-dimethyl-1,7-dihydrodipyrazolo[3,4-b;4′3′-e]pyridine (PAP-CB). Yield: 81.1%. mp 311−313 °C. ^{1}H NMR (δ, $CDCl_3$): 2.27 (s, 6H), 7.27−7.37 (m, 4H), 7.48−7.49 (d, 4H), 7.52−7.57 (t, 4H), 7.72−7.82 (q, 4H), 8.17−8.20 (d, 2H), 8.42−8.45 (d, 4H). FAB mass (*m*/*z*): 580 (M^+). Anal. Calcd for $C_{39}H_{28}N_6$: C, 80.67; H, 4.86; N, 14.47. Found: C, 80.81; H, 4.66; N, 14.48%.

The TPBI was prepared from benzene-1,3,5-tricarbonyl chloride and *N*-phenyl-1,2-phenylenediamine, followed by dehydration.[14] The NPB and AlQ were prepared via published methods. All charge-transporting materials were subjected to gradient sublimation twice prior to use. The substrate was an indium tin oxide (ITO)-coated glass with a sheer resistance of ∼50 $\Omega\square^{-1}$.

Device Fabrication. Pre-patterned ITO substrates with an effective individual device area of 3.14 mm^2 were cleaned by sonication in a detergent solution for 3 min and then washed with a large amount of doubly distilled water. Further sonication in ethanol for 3 min was done before blowing dry with a stream of nitrogen. The ITO substrates were then treated with oxygen plasma for 1 min before being loaded into the vacuum chamber. The organic layers were deposited thermally at a rate of 0.1−0.3 nm/s under a pressure of ∼2 × 10^{-5} Torr in an Ulvac Cryogenic deposition system. Typical devices were constructed with 40 nm of NPB as the hole-transporting layer (HTL), 10 nm of PAP-X as the emission layer, and 30 nm of AlQ or TPBI as the ETL. An alloy of

(12) Ganesan, A.; Heathcock, C. H. *J. Org. Chem.* **1993**, *58*, 6155.
(13) Puchala, A.; Rasala, D.; Kolehmainen, E. *OPPI BRIEFS* **1997**, *29*, 212.
(14) (a) Shi, J.; Tang, C. W.; Chen, C. H. U.S. Patent, 5,645,948, 1997. (b) Chen, C. H.; Shi, J. *Coord. Chem. Rev.* **1998**, *171*, 161.

Scheme 1

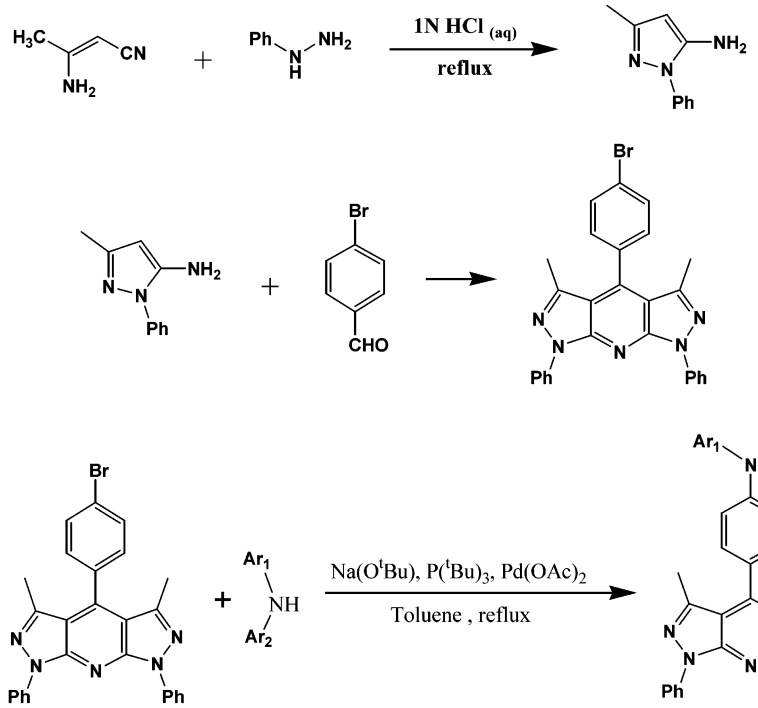

Table 1. Absorption, Emission, and Electrochemical Data of PAP-X Derivatives

compound	MW	λ_{max}, nm (CH_2Cl_2)	λ_{em}, nm (CH_2Cl_2)	λ_{em}, nm (solid film)	T_g, °C	Q.Y., %	HOMO/LUMO, eV	band gap, eV
PAP-NPA	632.75	261, 280 333, 365	490	460	102	53	5.60/2.72	2.88
PAP-DTA	610.75	260, 280 327, 373	520	474	97	42	5.44/2.61	2.83
PAP-DPA	582.70	260, 280 330, 361	494	458	87	52	5.59/2.73	2.86
PAP-CB	580.67	259, 280 329, 377	454	454	119	51	5.97/3.00	2.97

magnesium and silver (ca. 10:1, 50 nm) was deposited as the cathode, which was capped with 100 nm of silver. The current−voltage−luminance was measured in ambient conditions with a Keithley 2400 Source meter and a Newport 1835C Optical meter equipped with 818ST silicon photodiode.

Results and Discussion

The synthesis of the four derivatives are outlined in Scheme 1 from a common intermediate, the 4-bromophenyl-1,7-diphenyl-3,5-dimethyl-1,7-dihydrodipyrazolo [3,4-b;4′,3′-e]pyridine. The palladium-catalyzed reaction gave 70−80% yield of analytically pure products. For device fabrication, the materials were further sublimed twice through a gradient sublimator.

Thermal Properties. The PAP dyes here possess high melting points (~250 °C and above). Differential scanning calorimetry (DSC) measurements showed that a glass transition temperature, T_g, between 87 and 119 °C was observed for these four compounds and the T_g increases in the order PAP-DPA < PAP-DTA < PAP-NPA < PAP-CB (Table 1). While the first three compounds exhibited a typical crystallization phase change after the amorphous material was heated beyond T_g, the PAP-CB exhibited two crystallization peaks beyond T_g, which may be associated with two different crystal phases.[15] In general, the triarylamine group indeed helps to induce/raise the T_g in this series of PAP derivatives.[11,15] A similar effect was also observed in several other series.[16]

Optical Properties. The UV absorption spectra were taken in CH_2Cl_2 and are shown in Figure 2, with the λ_{max} values collected in Table 1. The same spectral pattern was observed for differently substituted derivatives. Strong absorption occurs in the range of 250−450 nm. In contrast, only one emission peak was observed in the photoluminescence (PL) spectra of these PAP-X dyes in CH_2Cl_2 and the peak positions are also listed in Table 1. The quantum yields using Coumarin 1 as the reference are rather similar, in the range around 50%. The solid-state PL spectra were measured for thin films of PAP dyes evaporated on a glass substrate (Figure 3). They are blue-shifted relative to the PL in CH_2Cl_2 solution except for the carbazolyl-substituted one, which has the same λ_{max}. Molecular simulation (using the Spartan Pro program) indicates that, in PAP-DPA, PAP-DTA, and PAP-NPA, the freely rotating aryl groups can approach a coplanar geometry around the nitrogen, whereas in the rigid carbazolyl-substituted case, the nitrogen is not planar. This will affect the conjugation between the triaryl moiety and the dipyrazolo moiety

(15) Shirota, Y. *J. Mater. Chem.* **2000**, *10*, 1.
(16) (a) Justin Thomas, K. R.; Lin, J. T.; Tao, Y. T.; Ko, C. W. *Chem. Mater.* **2002**, *14*, 1354. (b) Justin Thomas, K. R.; Lin, J. T.; Tao, Y. T.; Chuen, C. H. *Chem. Mater.* **2002**, *14*, 2796.

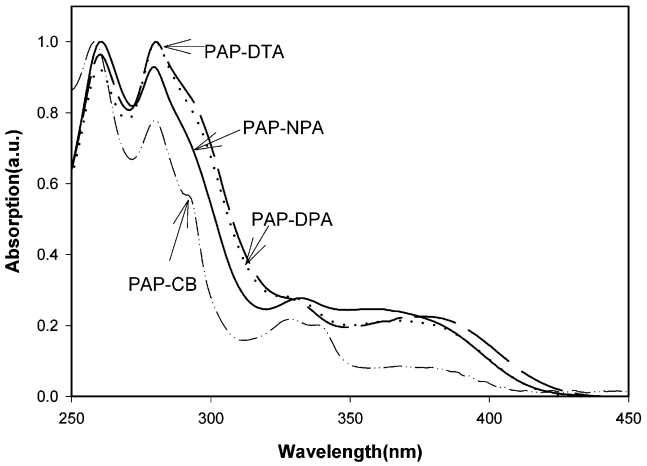

Figure 2. UV absorption of the PAP-X derivatives in CH_2Cl_2.

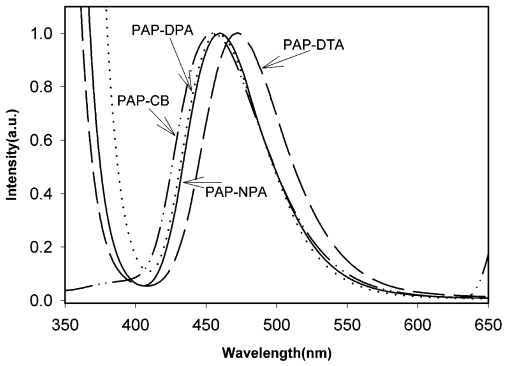

Figure 3. Normalized photoluminescence spectra of PAP-X materials in the solid film state.

so that little solvent effect on the emission maximum occurs for PAP-CB as compared to the other three. The staggered ring system also discourages the stacking of the molecule so that strong fluorescence is exhibited by all these dyes in the solid state.

Electrochemistry. All four PAP dyes exhibit an irreversible oxidation peak at the glassy carbon electrode at potentials around 1.0−1.3 eV relative to the Ag/AgCl electrode. The oxidation potential is clearly lower than that of the substituted PAP dyes reported earlier (∼1.56 eV),[11] presumably because of the involvement of the lone-pair electrons with the amino group during oxidation. A substituent effect is clear in that the oxidation potential increases as such, PAP-DTA < PAPPAP-NPA ∼ PAP-DPA < PAP-CB, which reflects the electron density of the aryl groups on the nitrogen atom.

The HOMO energy level is correlated to the oxidation potential according to the equation[17] that IP = (E_{OX} + 4.4) eV and the LUMO energy level is obtained by subtraction of the optical band gap from the IP. The results are listed in Table 1. The PAP-CB exhibits the lowest HOMO and LUMO and the PAP-DTA has the highest. Thus, the substituent has a similar effect on LUMO as on HOMO.

Electroluminescence. The strong fluorescence exhibited by the PAP-X dyes both in solution as well as

(17) (a) Agrawal, A. K.; Jenekhe, S. A. *Chem. Mater.* **1996**, *8*, 579. (b) Janietz, S.; Bradley, D. D. C.; Grell, M.; Giebeler, C.; Inbasekaran, M.; Woo, E. P. *Appl. Phys. Lett.* **1998**, *73*, 2453.

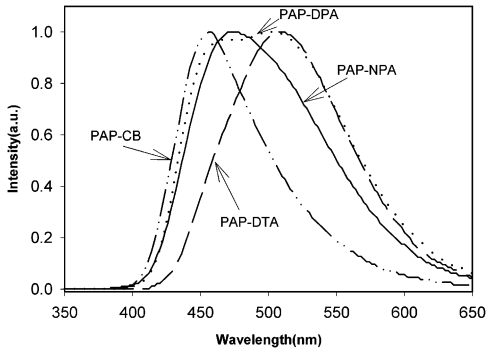

Figure 4. Normalized electroluminescence spectra of ITO/NPB/PAP-X/AlQ/Mg:Ag devices. The applied voltage was around 8 V.

in solid state suggests these materials are suitable candidates for fabricating a light-emitting device. A three-layer device configuration was examined, where the PAP-X dyes were used as the emission layer and the NPB was the hole transporter. Either AlQ or TPBI was used as the electron transporter. The results are discussed separately.

(a) ITO/NPB/PAP-X/AlQ/Mg:Ag Devices. With the same configuration of ITO/NPB(40 nm)/PAP-X(10 nm)/AlQ(30 nm)/Mg:Ag(50 nm), a bright blue or blue-green emission was obtained. Figure 4 depicts the normalized EL spectra of all four devices. In a comparison with the PL spectra of vacuum-deposited films of the dyes, some deviation was observed. For PAP-CB, a blue emission at 458 nm with a full-width at half-maximum (fwhm) of 76 nm was obtained. This closely matches that of the solid film PL of this compound, suggesting dye emission as the major component in EL. For PAP-NPA, a much broader emission peaking at 474 nm was obtained. In the case of PAP-DPA, clearly two peaks at 466 and 502 nm were obtained in EL. Whereas for PAP-DTA, the emission occurred at 508 nm, shifted by 34 nm from the corresponding PL for the solid film of PAP-DTA. All four EL spectra were found to be a composite of the PL spectra of AlQ and respective dye in different proportions. Thus, the result is interpreted as a broader recombination area, with various amounts of contribution from the AlQ emission in the EL spectra. A deconvolution of the PL spectra showed that the AlQ contribution in the EL spectra increases in the order PAP-CB < PAP-NPA < PAP-DPA < PAP-DTA. An analysis of the energy level alignment of various layers involved in the device (Figure 5a) indicates that the barrier for electron crossing from AlQ to the dye layer is the lowest for PAP-CB and is the highest for PAP-DTA, even though the barrier for hole crossing from the dye layer to AlQ is also the lowest for PAP-CB and the highest for PAP-DTA. The observation that PAP-CB emission is the major component in the EL spectrum of a PAP-CB-based device whereas AlQ emission is the major component in the EL spectrum of a PAP-DTA-based device implies that electrons were arriving at the dye/AlQ interface earlier than the holes. Thus, the ability of electron crossing into the LUMO of the dye layer is determining the whereabouts of the recombination region. With a smaller barrier, such as in the case of PAP-CB, the electrons can cross into the dye layer readily and recombine with the approaching holes mainly inside the dye layer to give mainly the dye

Table 2. Performances of Various PAP-X-Based Devices

devices structure	turn-on voltage[a] (V)	at 100 mA/cm^2 V	brightness, cd/m^2	Q.E.	luminescence efficiency, cd/A	power efficiency, lm/W	λ_{em}	C.I.E.	max. brightness	max. Q.E., %
NPB/PAP-CB/Alq	3.7	7.34	928	0.65	0.93	0.40	458	(0.17,0.17)	6231	0.65
NPB/PAP-CB/TPBI	3.8	6.81	775	0.84	0.77	0.36	450	(0.15,011)	5543	0.84
NPB/PAP-DPA/Alq	3.4	5.82	2992	1.30	2.98	1.61	502	(0.23,0.34)	23319	1.32
NPB/PAP-DPA/TPBI	3.3	6.98	1782	1.87	1.78	0.80	456	(0.14,0.11)	13375	2.00
NPB/PAP-DTA/Alq	3.3	5.70	3253	1.23	3.24	1.79	508	(0.25,0.43)	29702	1.30
NPB/PAP-DTA/TPBI	3.1	5.27	2335	1.71	2.33	1.38	468	(0.14,0.18)	21063	2.11
NPB/PAP-NPA/Alq	3.6	5.95	3653	1.64	3.66	1.94	474	(0.21,0.31)	35292	1.70
NPB/PAP-NPA/TPBI	3.3	6.29	2673	2.76	2.67	1.34	456	(0.15,0.11)	20679	2.76

[a] Defined as the voltage at which a luminance of 1 cd/m^2 was obtained.

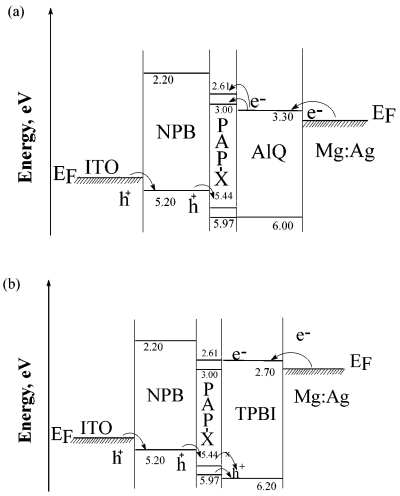

Figure 5. Energy alignment and charge flow in (a) ITO/NPB/PAP-X/AlQ/Mg:Ag and (b) ITO/NPB/PAP-X/TPBI/Mg:Ag devices.

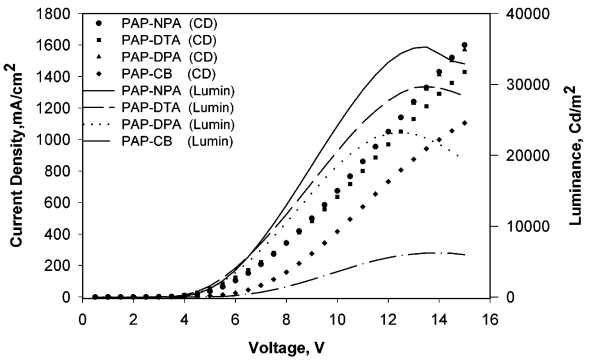

Figure 6. Current−voltage−luminance characteristics of ITO/NPB/PAP-X/AlQ/Mg:Ag devices.

emission. With a larger barrier imposed, such as the case of PAP-DTA, the electrons will be stopped at the interface and instead the holes can pass to the ETL and recombine with the electrons accumulated at the interface to give mainly the AlQ emission. For PAP-DPA and PAP-NPA, the barriers are intermediate; contributions from both the dye and AlQ are significant.

The current−voltage−luminance plots for these AlQ-based devices are shown in Figure 6, with specific performance data summarized in Table 2. The turn-on voltages (defined as the voltage at which a luminance >1 cd/m^2 was observed) for PAP dyes are lower than ∼4 V. The operating voltage at a current density of 100 mA/cm^2 shows a substituent dependence: PAP-DTA < PAP-DPA ∼ PAP-NPA < PAP-CB. Referring to the energy level alignment diagram (Figure 5), this appears

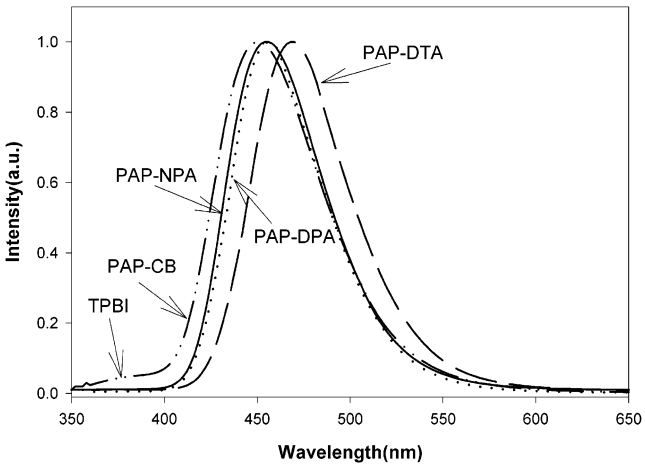

Figure 7. Normalized electroluminescence spectra of ITO/NPB/PAP-X/TPBI/Mg:Ag devices. The applied voltage was around 8 V.

to parallel the hole-crossing barrier from NPB to the dye layer. The brightness ranges between 900 and 3700 cd/m^2 at a driving current of 100 mA/cm^2. The luminance efficiency also shows a substituent effect, increasing from 0.9 cd/A for a PAP-CB-based device to 3.66 cd/m^2 for a PAP-NPA-based device. The lower external quantum efficiency reflects a greatly unbalanced charge recombination.[18] The improved quantum efficiency in going from PAP-CB to PAP-DTA suggests that the unbalance is less severe (thus quantum efficiency increases). The PAP-CB gave the lowest external quantum efficiency and the barrier for hole crossing at the NPB/dye interface is also the highest. The aggravated charge unbalance associated with PAP-CB might imply that, at the dye/AlQ interface, there are more electrons than the holes. (It is noted that the electrons are generally considered to be the minor carrier in a standard NPB/AlQ device.[19] However, with the three-layer device here involving the dipyrazolo dye, the situation may be different.)

(b) ITO/NPB/PAP-X/TPBI/Mg:Ag Devices. Figure 7 shows the normalized EL spectra of ITO/NPB(40 nm)/PAP-X(10 nm)/TPBI(30 nm)/Mg:Ag(50 nm) devices. A comparison of the PL and the EL spectra confirms that the emissions came from the dye layer in the device. Nevertheless, a small shoulder at around 380 nm due to TPBI emission[20] was observed for a PAP-CB-based

(18) Khramtchenkov, D. V.; Bassler, H.; Arkhipov, V. I. *J. Appl. Phys.* **1996**, *79*, 9283.
(19) Naka, S.; Okada, H.; Onnagawa, H.; Yamaguchi, Y.; Tuutsui, T *Synth. Met.* **2000**, *111*−*112*, 331.

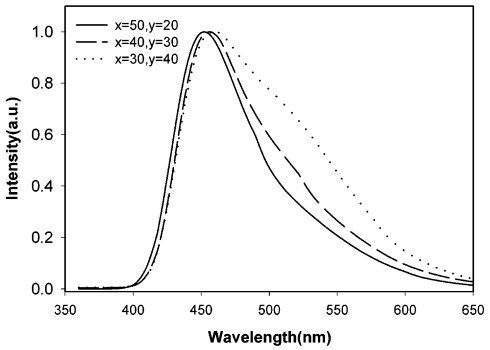

Figure 8. EL spectra of ITO/NPB/PAP-NPA/AlQ/Mg:Ag devices as a function of layer thickness.

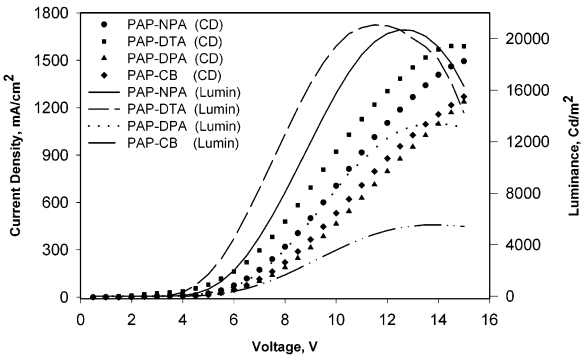

Figure 9. Current−voltage−luminance characteristics of ITO/NPB/PAP-X/TPBI/Mg:Ag devices.

device. A substituent-dependent hole leakage was also observed in a previous series of PAP dyes.[11] An analysis of the energy alignment (Figure 5b) reveals that the barrier for hole leakage to the TPBI layer is the lowest for a PAP-CB-based device, even though the electron crossing from the TPBI layer to the dye layer is most facile. The fact that other dyes with a higher electron-crossing barrier than that for PAP-CB did not give any TPBI emission implies that the holes were arriving at the dye/TPBI interface earlier than the electrons were and the ease for hole crossing into TPBI determines the amount of hole leakage and thus TPBI contribution. TPBI has served as a hole blocker in many cases due to its low-lying HOMO.[20,21] Only in the case of a dye with low-lying HOMO will there be hole leakage into the TPBI, giving TPBI emission. This is in contrast with the AlQ-based devices above. The different timing for the charges arriving at the interface may relate to a different electron mobility for the two electron transporting materials.[22] The electron mobility is higher in AlQ, the electrons reach the dye/AlQ interface faster, and the electron-crossing barrier from AlQ to the dye layer determines the amount of AlQ contribution in the EL. It is contemplated that increasing the thickness of the AlQ layer would slow the timing for electrons reaching the interface and shift the recombination region deeper into the AlQ layer. An increasing contribution from AlQ emission would result, whereas reducing the thickness of AlQ and increasing the thickness of NPB would expedite the timing for electrons reaching the interface and increase the contribution of the dye emission. Figure 9 shows the EL spectra of devices with a systematic change in thickness of AlQ and NPB while maintaining a constant total thickness. The contribution of AlQ emission indeed increased with increasing thickness of AlQ. (It is noted that similar field and film thickness dependence on the electroluminescence was observed in a bilayer polymer device and was interpreted in terms of charge carrier range.[23]) In the case where TPBI is the ETL, the electron mobility was lower, the holes reached the dye/TPBI interface earlier, and the barrier for hole crossing from the dye to the TPBI layer determined the contribution of TPBI in the EL spectra.

Nearly pure blue emission was observed for all dyes in the TPBI-based devices, except PAP-DTA, which shifts slightly to the green (Figure 7). The CIE *x,y* coordinates and other performance characteristics are collected in Table 2. Figure 9 shows the I−V−L characteristics for the four devices. Again, turn-on voltages lower than 4 V were observed and depends on the substituent: increasing from 3.1 V for PAP-DTA to ∼3.3 V for PAP-DPA and PAP-NPA to 3.8 V for PAP-CB. The trend roughly parallels the barrier for hole crossing from the NPB layer to the dye layer. At a driving current of 100 mA/cm^2, the external quantum efficiency increases from 0.84% for PAP-CB to 2.76% for PAP-NPA. The luminance efficiency reaches 2.67 cd/A for a PAP-NPA-based device. A maximum brightness of more than 20 000 cd/m^2 was obtained for two of the devices. Considering the purity of the color, these are very promising bright blue devices.

Conclusions

In conclusion, a new series of dipyrazolopyridine dyes were synthesized and used as the emitting material in fabricating EL devices. Very bright blue or blue-green emission from the dye can be obtained in a double-heterojunction device structure with NPB as the HTL and either AlQ or TPBI as the ETL. The electroluminescence behavior depends on the substituent as well as the ETL used due to a subtle shift in the recombination region. The change results from different electron mobility of the ETL as well as barriers for the charge crossing. With AlQ as the ETL, electrons reach the dye/ETL interface ahead of the holes and the barrier for electron injection across the interface determines the recombination region and thus purity of the color. While with TPBI as the ETL, the holes reach the dye/TPBI interface first and the barrier for hole crossing to TPBI determines the purity of the color. Several of the derivatives offer nearly pure blue emission with good luminance efficiency and very high brightness.

Acknowledgment. Financial support from Academia Sinica, Republic of China, is gratefully acknowledged.

CM020284H

(20) Tao, Y. T.; Balasubramaniam, E.; Danel, A.; Tomasik, P. *Appl. Phys. Lett.* **2000**, *77*, 933.

(21) (a) Tao Y. T.; Balasubramaniam, E.; Tomasik, P.; Danel, A.; Jarosz, B. *App. Phys. Lett.* **2000**, *77*, 1575. (b) Zhilin, Z.; Xueyin, J.; Shaohong, X. *Thin Solid Films* **2000**, *363*, 61.

(22) The electron mobility of TPBI was reported to be in the range of 10^{-6}–10^{-5} cm^2/V s and is "comparable" to that of AlQ: Wong, T. C.; Kovac, J.; Lee, C. S.; Hung, L. S.; Lee, S. T. *Chem. Phys. Lett.* **2001**, *334*, 61. The two have different sensitivities toward electric field though.

(23) (a) Jenekhe, S. A.; Zhang, X.; Chen, X. L.; Choong, V. E.; Gao, Y. Hsieh, B. R. *Chem. Mater.* **1997**, *9*, 409. (b) Zhang, X.; Jenekhe, S. A. *Macromolecules* **2000**, *33*, 2069.